Numerical integration of the gasdynamic equations

T. H. Chong and L. Sirovich[a)]

Applied Science Research Associates, Inc., New York, New York 10023
(Received 25 January 1979; accepted 18 April 1980)

The gasdynamic equations are transformed to new coordinates based on particle paths and an appropriate set of characteristics. The numerical integration of the transformed equations is accomplished by a scheme which is accurate, rapidly convergent, and free from shock oscillations. Complete flow solutions are presented in graphical form for several cases.

I. INTRODUCTION

In this paper we furnish exact numerical solutions of the gasdynamic equations following the techniques developed by Sirovich and Chong[1] [hereafter referred to as (I)].

The class of problems considered is one-dimensional unsteady flows. In addition to being interesting in their own right, such problems have a long history as a proving ground of methods for the numerical integration of the gasdynamic equations.[2] For the most part the "brute force" approach has been used in these methods. By this, one means that the partial differential equations of gasdynamics are treated directly. A discussion of the various methods then reduces to a discussion of differencing schemes, e.g., Lax,[3] Rusanov,[4,5] Lax-Wendroff,[6] MacCormack,[7] and Godunov.[8] A review of these techniques applied to the problems under consideration has been given by Moretti[9,10] and Taylor *et al.*[11] In this connection mention should also be made of the random sampling approach taken by Chorin[12] which in turn is based on work by Glimm.[13]

The brute force method suffers from a number of chronic ailments. Chief among these are slow convergence, oscillations or wiggles (especially near discontinuities), and shocks which are poorly defined as a result of numerical viscosity. The method of characteristics,[14] which is better grounded both mathematically and physically, has been proven to be too cumbersome and formidable for practical use. Hoskin and Lambourne,[15] however, have, at least in one instance, demonstrated the superiority of the method of characteristics to the brute force method.

II. RESUMÉ OF THE EQUATIONS

We briefly summarize the gasdynamics equations as derived in (I). The variables (x,t) are transformed to a new system $\alpha(x,t)$, $\beta(x,t)$, such that α is a constant on particle paths and β is a constant on C^+ characteristics

$$\frac{\partial\alpha}{\partial t}+u\frac{\partial\alpha}{\partial x}=0,\quad C^+\colon\ \frac{\partial\beta}{\partial t}+(u+c)\frac{\partial\beta}{\partial x}=0\,. \tag{1}$$

Because entropy is constant on particle paths, $S=S(\alpha)$. The two momentum equations become

$$r^+_\alpha=(c/\gamma)S_\alpha\,, \tag{2}$$

$$r^-_\beta=t_\beta(u_\alpha/t_\alpha)\,, \tag{3}$$

where $r^\pm=u\pm 2c/(\gamma-1)$ are the positive and negative Riemann invariants.

The transformation back to the physical plane is given by

$$t(\alpha,\beta)=t(0,\beta)+\int_0^\alpha \frac{A(\alpha')\,d\alpha'}{[c(\alpha',\beta)]^{(\gamma+1)/(\gamma-1)}}\,, \tag{4}$$

$$x=P(\beta)+\int_0^\alpha [u(\alpha',\beta)+c(\alpha',\beta)]t_\alpha(\alpha',\beta)\,d\alpha'\,. \tag{5}$$

We fix one of the arbitrary functions by

$$t(0,\beta)=\beta\,. \tag{6}$$

It then follows that $P(\beta)$ is the piston path $x=P(t)$ evaluated at $t=\beta$.

In addition to Eqs. (1)–(6) we have the usual shock relations. If we write the shock trajectory as

$$\frac{dx}{dt}=M\,, \tag{7}$$

where M is the Mach number of the shock, then at the lead shock,

$$S=\frac{1}{\gamma-1}\ln\left[\left(1+\frac{2\gamma}{\gamma+1}(M^2-1)\right)\times\left(\frac{1+[(\gamma-1)/(\gamma+1)](M^2-1)^\gamma}{M^2}\right)^\gamma\right]. \tag{8}$$

$$r^+=\frac{2}{\gamma+1}\left(\frac{M^2-1}{M}\right)+\frac{2}{\gamma-1}\left[1+\frac{2(\gamma-1)}{(\gamma+1)^2}\left(\frac{\gamma M^2+1}{M^2}\right)(M^2-1)\right]^{1/2}, \tag{9}$$

$$r^-=\frac{2}{\gamma+1}\left(\frac{M^2-1}{M}\right)-\frac{2}{\gamma-1}\left[1+\frac{2(\gamma-1)}{(\gamma+1)^2}\left(\frac{\gamma M^2+1}{M^2}\right)(M^2-1)\right]^{1/2}. \tag{10}$$

In the (α,β) plane, instead of (9) we have

$$t_\alpha+\beta'(\alpha)\left(\frac{u-M}{u-M+c}\right)t_\beta=0\,, \tag{11}$$

where $\beta(\alpha)$ is the shock trajectory in the (α,β) plane and all quantities in (13) are evaluated at $\beta=\beta(\alpha)$. Equation (11) with (4) yields

a)Permanent address: Division of Applied Mathematics, Brown University Providence, R.I. 02912.

 0031-9171/80/071296-05$00.90

$$0 = 1 + \frac{A(\alpha)(u - M + c)}{c^{(\gamma+1)/(\gamma-1)}\beta'(\alpha)(u - M)}$$

$$+ \int_0^\alpha A(\alpha') \frac{\partial}{\partial \beta} [c(\alpha', \beta)^{-(\gamma+1)/(\gamma-1)}] d\alpha' . \quad (12)$$

Equation (12) is evaluated at the shock $\beta = \beta(\alpha)$, which then determines $A(\alpha)$.

III. METHOD OF SOLUTION

The governing equations are solved by an iteration procedure starting with a relatively accurate approximate solution as given in (I).

A. Grid system

For the exact numerical integration we fix the shock in the (α,β) plane to be that given by the approximate solution. This has the decided advantage that the shock does not change with iteration.

For the numerical calculation, we construct a grid system in the (α,β) plane as follows: A constant grid size in α is chosen. The shock trajectory $\beta = \beta(\alpha)$ then determines the grid sizes (nonuniform) for $0 \leq \beta \leq 1$ (see Fig. 1). For $\beta > 1$, we return to a uniform grid in β which is the same size as the last β-grid size just before $\beta = 1$. Since the shock trajectory $\beta = \beta(\alpha)$ is slowly varying (see Fig. 1), the grid sizes for $0 \leq \beta \leq 1$ will also be slowly varying and will not adversely affect the error estimate of the finite difference scheme.[16] The tail shock, indicated by a dashed line in Fig. 1, does not enter directly into the calculation and is included for reference only.

B. Iteration procedure

The steps of the iteration procedure are indicated in the flow diagram, Fig. 2. In somewhat more detail these steps are the following:

Step 1. r^- at the shock, Eq. (10), is computed using the current solution (the approximate solution is used at first iteration). This gives the initial data for the solution of (3), which is formally

$$r^-(\alpha,\beta) - r^-[\alpha,\beta(\alpha)] = \int_{\beta(\alpha)}^{\beta} \frac{t_\beta}{t_\alpha} u_\alpha \, d\beta . \quad (13)$$

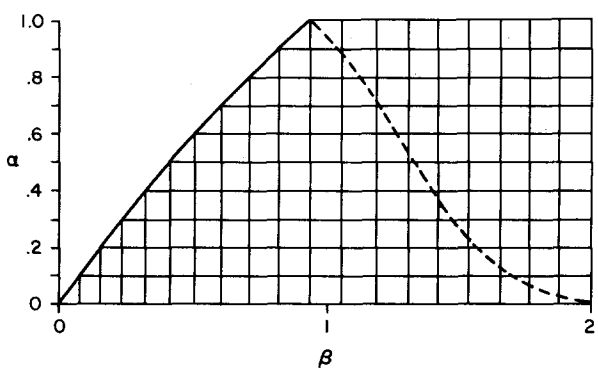

FIG. 1. Grid structure in the (α,β) plane. The α axis is uniformly divided; the β divisions are determined by the intersections with the shock curve at the left. A nominal number of grid points are shown. In actual practice the α axis has roughly 100 divisions.

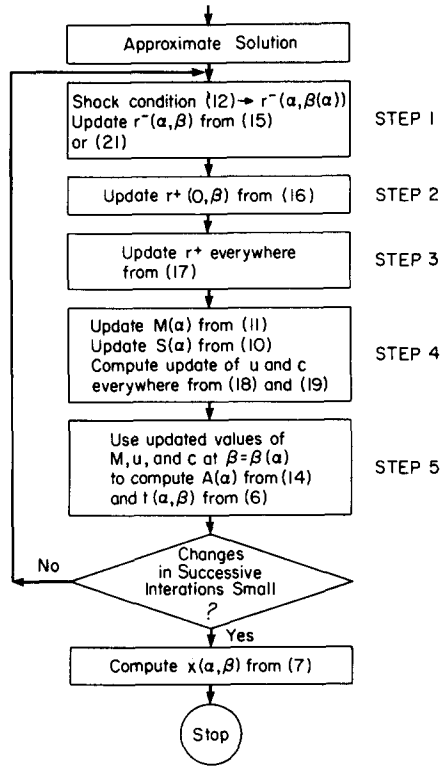

FIG. 2. The flow diagram for the numerical procedure.

The current values of t and u (approximate solution at first iteration) are used on the right-hand side of (13).

Step 2. Use step 1 to update r^+ at the piston

$$r^+(0,\beta) = 2P'(\beta) - r^-(0,\beta) . \quad (14)$$

Step 3. Formally integrate (2) to update $r^+(\alpha,\beta)$

$$r^+(\alpha,\beta) = r^+(0,\beta) \exp\left(\frac{\gamma-1}{4\gamma}[S(\alpha) - S_0]\right)$$

$$+ \int_0^\alpha r^-(\alpha',\beta) \frac{d}{d\alpha'} \exp\left(\frac{\gamma-1}{4\gamma}[S(\alpha) - S(\alpha')]\right) d\alpha' , \quad (15)$$

where $r^+(0,\beta)$ is obtained from step 2, $r^-(\alpha,\beta)$ from step 1, and S is the current value (approximate solution at first iteration).

Step 4. Use current $r^+[\alpha,\beta(\alpha)]$ to update $M(\alpha)$ from Eq. (9). Then, use (8) to obtain update of $S(\alpha)$. u and c are then computed from current values of $r^\pm$

$$u(\alpha,\beta) = \tfrac{1}{2}[r^+(\alpha,\beta) + r^-(\alpha,\beta)] , \quad (16)$$

$$c(\alpha,\beta) = [(\gamma-1)/4][r^+(\alpha,\beta) - r^-(\alpha,\beta)] . \quad (17)$$

Step 5. Use current values of M, u, and c at shock, $\beta = \beta(\alpha)$, in Eq. (12) to compute $A(\alpha)$. Equation (4) gives $t(\alpha,\beta)$.

Subject to a convergence criterion (which is to be discussed), we either reiterate or exit and compute $x(\alpha,\beta)$ from (5).

C. Finite differences

A second-order finite differencing scheme is used throughout the numerical calculation; the trapezoidal rule for integration and three-point schemes on all derivatives. No interpolation is required since the shock and, hence, the grid is fixed.

D. Stability of iterations

The iteration scheme as just presented was found to exhibit oscillations which grew or decayed depending on conditions of the problem. The oscillations, growing or decaying, were regular and predictable. We found that the method of accelerated convergence[17] could be used to force convergence even in the case of growing oscillations. However, in examining the causes of oscillation and the lack of convergence, we developed other more direct methods.

The chief cause for the oscillation arises in the computation of r^-, the negative Riemann invariant. This quantity was uniformly overestimated or underestimated at each iteration. We recall that r^- is computed from (3) by integration along $\alpha = \text{const}$, i.e., particle paths in the physical plane. A different determination of r^- follows if we replace (3) by

$$\frac{\partial}{\partial \alpha} r^- = 2u_\alpha - \frac{c}{\gamma} S_\alpha \tag{18}$$

which is obtained by rearranging (2) and (3). If (19) is integrated, we obtain

$$r^-(\alpha,\beta) = r^-[\alpha(\beta),\beta] - \int_{\alpha(\beta)}^{0} \left(2u_\alpha - \frac{c}{\gamma} S_\alpha\right) d\alpha\,, \tag{19}$$

where $\alpha = \alpha(\beta)$ is the shock. Regular oscillations again occur. However, in this case, the oscillations are out-of-phase with those in the previous case.

On both physical and mathematical grounds, we know that the variation of r^- is more appropriately computed

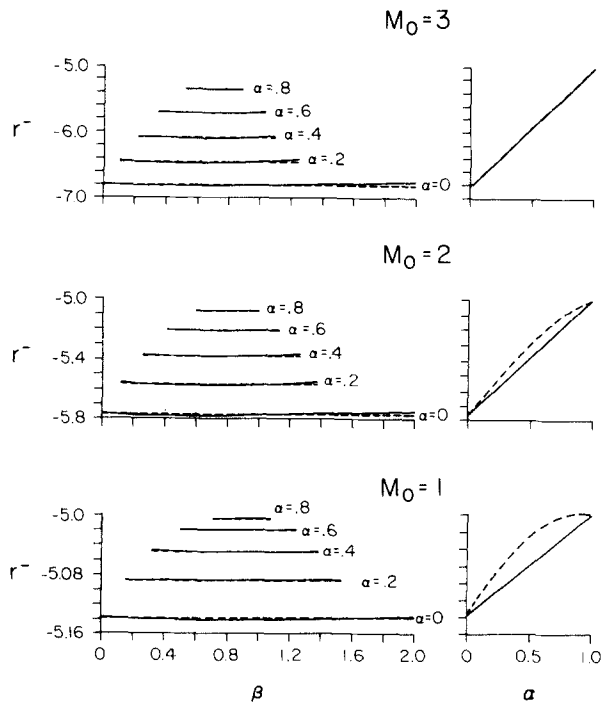

FIG. 3. Backward Riemann invariant. The solid lines at the left give r^- versus β on the particle paths, $\alpha = \text{const}$. Dashed lines indicate average values of r^-. At the right, for each case, the average value of r^-, on $\alpha = \text{const}$, is plotted versus α (dashed line); also included is a plot of Eq. (24) (solid line).

along negative-going characteristics: C^-: $dx/dt = u - c$, which in the physical plane represents waves reflected from the shock. The appropriate equation to integrate is

$$\left(\frac{\partial}{\partial \alpha} - \frac{2t_\alpha}{t_\beta}\frac{\partial}{\partial \beta}\right) r^- = -\frac{c}{\gamma} S_\alpha\,. \tag{20}$$

Integration of Eq. (20) is awkward since C^- trajectories do not necessarily fall on grid points and, in any case, change with iteration. In view of this difficulty, we mo-

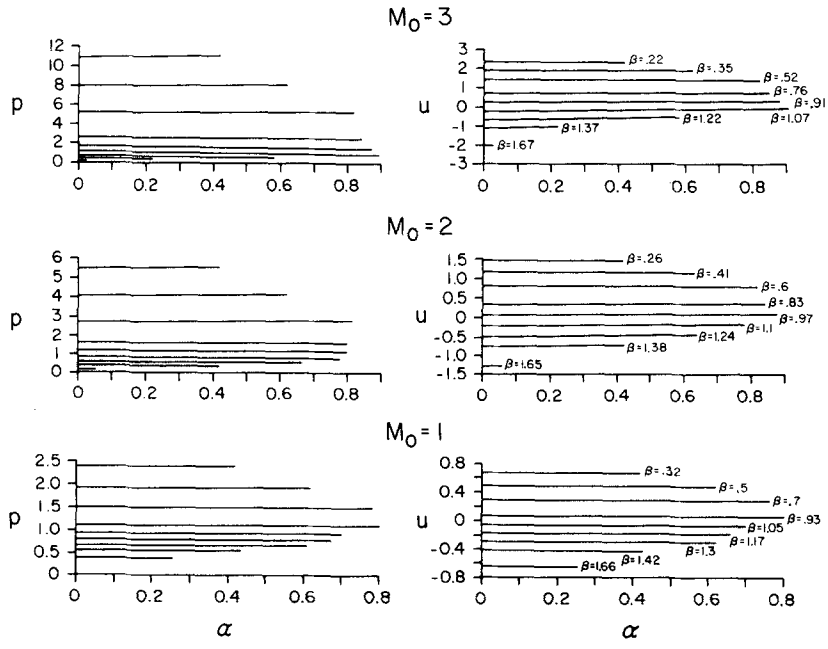

FIG. 4. Pressure and fluid velocity. Graphs are given of pressure p and velocity u versus α on C^+ characteristics. The C^+ characteristics are indicated by their β values. The same sequence of β values apply to the curves at the left. Each curve is, to good approximation, an almost horizontal straight line.

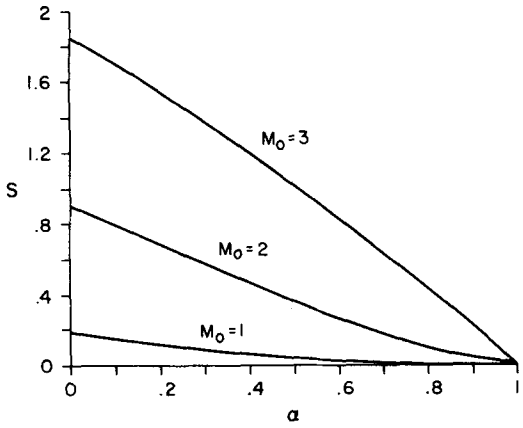

FIG. 5. Entropy variation.

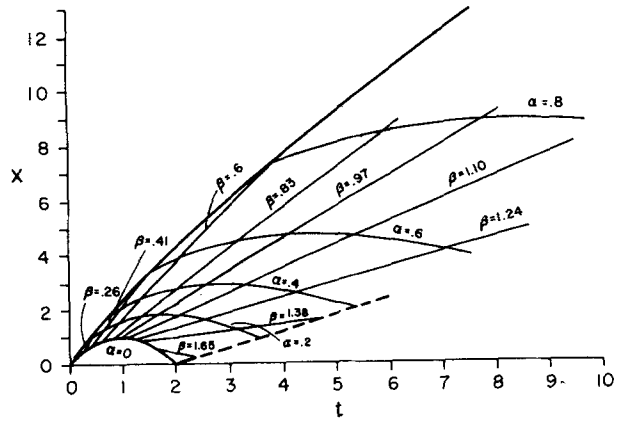

FIG. 7. C^+ characteristics and particle paths in the physical plane: $M_0=2$ (see Fig. 6).

del the integration along C^- by taking a mean value of (13) and (19) (the mean is based on the average direction of C^-). This should cause no concern, for in a convergent solution both (13) and (19) are valid questions.

The actual iteration was not always performed on the entire grid of Fig. 1, but rather on blocks of grid points. We divided the grid structure of Fig. 1 into roughly ten blocks treating each of these blocks as a separate numerical calculation and proceeding from the leftmost block to the right. Data for the current block is provided by the shock or the block to the left and the piston or the block below as the case requires. The reason for treating smaller blocks is twofold. Integration over the full grid produces an accumulated error which results in an iterated solution far from the actual solution on certain parts of the grid. Also, use of blocks can greatly reduce memory demands, which is of importance in large calculations.

E. Convergence of the numerical scheme

We performed the numerical calculations with a grid size $\Delta\alpha=0.02$, which puts 50 intervals between the piston, $\alpha=0$, and infinite, $\alpha=1$, (according to the approximate solution) and roughly 100 intervals in the β direction. For a 20×20 block each iteration took approximately 0.25 CPU sec on a DEC-20 computer. The number of iterations required for convergence depends on the Mach number of the piston, M_0, the block size, and, of course, the convergence criteria. For a 20×20 block and the convergence criterion that the maximum differences in u for three consecutive iterations be less than some tolerance, we have the following results: For $M_0=1$ and a tolerance of 10^{-6}, 12 iterations are required. If we change the tolerance to 10^{-4}, which is appropriate to the *a priori* error bound of our numerical scheme, the number of iterations is reduced to eight. For the case of $M_0=3$, the number of iterations required are 30 and 12 for tolerances of 10^{-6} and 10^{-4}.

The chief reason for slower convergence at higher Mach numbers is that the variation of t in the α direction (viz., t_α) becomes large at the end of the piston motion. This arises from the largeness of $|u|$ compared with $|c|$ near the end of the piston motion. Hence, the α and β characteristics which are defined by Eq. (1) are nearly parallel.

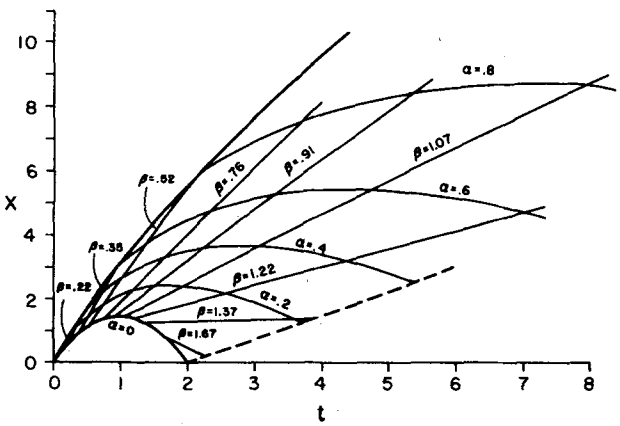

FIG. 6. C^+ characteristics and particle paths in the physical plane: $M_0=1$. Particle paths are indicated by their $\alpha=$const values and C^+ characteristics by their $\beta=$const values. The heavy solid curve is the leading shock and the dashed line is the trailing shock. The piston trajectory is given by $\alpha=0$.

IV. NUMERICAL RESULTS FOR A CLASS OF PARABOLIC PISTONS

We carried out extensive calculations for the case of parabolic pistons given by

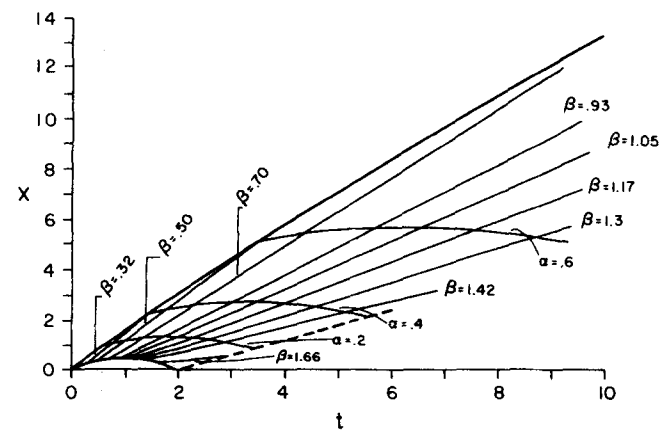

FIG. 8. C^+ characteristics and particle paths in the physical plane: $M_0=3$ (see Fig. 6).

$$x = P(t) = M_0 t(1 - t/2), \tag{21}$$

where M_0 is the initial Mach number of the piston. For $M_0 = 1$, 2, and 3, the Mach number of the generated shocks are 1.766, 2.762, and 3.860, and the corresponding entropy changes are 0.189, 0.911, and 1.856. Comparison between these cases and the approximate solution is, in part, given in (I). As was shown there, the shock trajectories as well as the pressure distributions on the piston are given quite accurately by the approximate theory. It should be noted that the $M_0 = 3$ case represents a considerable departure from equilibrium. In order to underline this, we note that in this case the temperature behind the initial shock is almost four times its upstream value. For further comparison we examine the "constancy" of r^- on particle paths. This is done in Fig. 3 where for each of the cases we plot r^- as a function of β on each of five particle paths as indicated. This is compared with the averaged value, the dashed line, and at the right the averaged values are plotted and compared with a straight line. All this suggests that

$$r^- \approx r_1^- + \alpha(r_0^- - r_1^-), \tag{22}$$

where r_0^- is the upstream value and r_1^- is the value behind the initial shock, provides an excellent approximation.

The relative constancy of r^- along particle paths has some interesting consequences. From (3) we have that $r_\beta^- = t_\beta u_\alpha / t_\alpha \approx 0$, which implies that u is slowly varying along C^+ characteristics, $\beta = \text{const}$. From this it follows that p is also slowly varying on C^+ [see (I), Eq. (17)]. This, in fact, is confirmed by our numerical solutions. In Fig. 4 we have plotted u versus α and p versus α on the C^+ characteristics for the three piston Mach numbers. The truncation of the line segments comes from intersection of the C^+ characteristics with the front or tail shocks. At higher Mach numbers, although slow variation is still a good approximation, there is a noticeable deviation from constancy.

The solutions in the (α,β) plane are completed by Fig. 5, which specifies $S(\alpha)$ for the three cases. Finally, the solutions in the physical plane are obtained, in graphic form, by exhibiting the $\alpha = \text{const}$ and $\beta = \text{const}$ characteristics in the physical plane. This is given in Figs. 6–8. On each of these, the numerically computed front shock as well as the α and β characteristics are shown. The tail shocks (dashed straight lines) are computed from the exact shock relations at the stopping point of the piston.

ACKNOWLEDGMENTS

This work was supported by the Office of Naval Research under Contract N00014-77-C-0359. Final preparation of this manuscript was done with the support of NASA Grant NSG-1617 with Brown University.

[1] L. Sirovich and T. H. Chong, Phys. Fluids **23**, 1291 (1980).
[2] P. J. Roache, *Computational Fluid Dynamics* (Hermosa, Albuquerque, N.M., 1976).
[3] P. D. Lax, Commun. Pure Appl. Math. **7**, 159 (1954).
[4] V. V. Rusanov, Zh. Vychisl. Mat. Mat. Fiz. **1**, 267 (1961). (National Research Council of Canada Technical Translation 1027).
[5] V. V. Rusanov, Fluid Dyn. Trans. **4**, 285 (1969).
[6] P. D. Lax and B. Wendroff, Courant Institute of Mathematical Sciences, New York University Report NYU 9759 (1962).
[7] R. W. MacCormack, presented at the AIAA Hypervelocity Impact Conference, Cincinatti, Ohio (1969).
[8] S. K. Godunov, Mt. Sb. **47**, 271 (1959).
[9] G. Moretti, Polytechnic Institute of Brooklyn PIBAL REport No. 71-25 (1971).
[10] G. Moretti, Polytechnic Institute of Brooklyn POLY-AE/AM Report No. 74-15 (1974).
[11] T. D. Taylor, E. Ndefo, and B. S. Masson, J. Comput. Phys. **9**, 99 (1972).
[12] A. J. Chorin, J. Comput. Phys. **22**, 517 (1976).
[13] J. Glimm, Commun. Pure Appl. Math. **10**, 537 (1957).
[14] H. W. Liepmann and A. Roshko, *Elements of Gasdynamics* (Wiley, New York, 1957).
[15] N. E. Hoskin and B. D. Lambourn, in *Proceedings of the 2nd International Conference on Numerical Methods in Fluid Dynamics*, edited by M. Holt (Springer–Verlag, Berlin, 1971), p. 230.
[16] T. H. Chong, SIAM J. Numer. Anal. **15**, 835 (1978).
[17] C. Brezinski, *Acceleration de la Convergence en Analyse Numerique* (Springer–Verlag, New York, 1977).